

## FROM LEO TO THE PLANETS USING WAVERIDERS

A. D. McDonald, J. E. Randolph  
 Jet Propulsion Laboratory  
 California Institute of Technology  
 M. J. Lewis  
 University of Maryland  
 E. P. Bonfiglio, J. Longuski  
 Purdue University  
 P. Kolodziej  
 Ames Research Center

ABSTRACT

A revolutionary interplanetary transportation technique known as Aero-Gravity Assist (AGA) has been studied by JPL and others to enable relatively short trip times between Earth and the other planets. It takes advantage of an advanced hypersonic vehicle known as a waverider that uses its high lift to fly through the atmospheres of Venus and Mars to provide exceptionally large velocity changes using gravity-assist maneuvers. The concept has been under study in a joint program between JPL and the University of Maryland for almost a decade. More recently Purdue University and NASA Ames Research Center have also become partners. The waverider concept has been proposed as an upper stage vehicle compatible with the Lockheed Martin Venture Star SSTO vehicle. This integrated vehicle concept could be used to launch spacecraft on interplanetary missions. The paper will discuss the mission possibilities enabled by a waverider vehicle as well as the necessary development program.

Flight durations to various destinations in the solar system can be reduced by large factors (e.g., 2-5 times shorter duration). The paper will present results of recent studies of interplanetary and atmospheric trajectories to many bodies, with navigation errors and make-up, of velocity loss at each AGA maneuver. Vehicle design includes possible ablation of heat shield material, and possible location and nature of

control surfaces, along with engines and propellant to escape from Earth. Other advantages of this technique over normal interplanetary delivery methods will be discussed.

INTRODUCTION AND BACKGROUND

The idea to employ the terrestrial planets as an energy source using aero-gravity-assist (AGA) maneuvers to significantly increase the velocity of interplanetary spacecraft was first discussed for the Starprobe mission to the sun<sup>1</sup> in 1982. Some preliminary analyses were then completed by Longuski<sup>2</sup> that suggested the necessity of a very high performance aerodynamic vehicle having a lift/drag (L/D) ratio of almost 10. This high performance at the extreme Mach numbers necessary for AGA maneuvers seemed unattainable at that time and the concept was not pursued. In the mid 1980s we became aware of an aerodynamic vehicle concept introduced by Nonweiler in the 1950s<sup>3</sup> which had been under study for some time at the University of Maryland.<sup>4</sup> The first public presentation of the AGA concept was made in 1989 by McDonald<sup>6</sup> and soon thereafter the connection between the AGA concept and waveriders was published by Lewis, et al<sup>7,8</sup> from the University of Maryland. This began a lengthy collaboration between JPL and the University of Maryland, which is ongoing today, and represents the nucleus of the team that continues to pursue the AGA idea for future interplanetary missions.

<sup>\*</sup> A.D. McDonald is a Senior Member of the Technical Staff, J.E. Randolph is the Study Manager for the Solar Probe, both at JPL, California Institute of Technology. M.J. Lewis is a Professor in the Department of Aerospace Engineering, University of Maryland, E. P. Bonfiglio is now a Member of the Technical Staff at JPL, and was previously a graduate student of Professor J. Longuski, who is at the School of Aeronautics and Astronautics, Purdue University, and P. Kolodziej is a Member of the Technical Staff at NASA Ames Research Center. The research described in this paper was carried out by the Jet Propulsion Laboratory, California Institute of Technology, under a contract with the National Aeronautics and Space Administration. The paper is to be presented at the AIAA 9th International Space Planes and Hypersonic Systems and Technologies Conference at Norfolk, VA on November 1-5, 1999.  
 Copyright 1990 by the American Institute of Aeronautics and Astronautics, Inc. The U.S. Government has a royalty-free license to exercise all rights under the copyright claimed herein for Governmental purposes. All other rights are reserved by the copyright owner.

More recent publications<sup>9,10,11</sup> document detailed investigations of actual AGA trajectories to various planets. Also, new analyses of specific waverider designs appropriate to CO<sub>2</sub> atmospheres (e.g., Venus and Mars) have led to more optimized waverider shapes. A model waverider based on these was tested in 1993 and the results<sup>13</sup> were very well predicted by the analytical codes.

Beginning in 1997, NASA first directly funded this research. This led to the formation of an AGA team consisting of Mark Lewis at the University of Maryland, James Longuski and Eugene Bonfiglio of Purdue University; and Angus McDonald, James Randolph, and Robert Miyake at JPL. One of the more significant products of this team effort was the development of a more detailed parametric "mission space" for AGA trajectories within the solar system using a new computer code. A program called STOUR<sup>14</sup> had been developed to parametrically study interplanetary trajectories with gravity assist maneuvers at intermediate planets. This program was modified by the team members at Purdue University to incorporate AGA maneuvers at each intermediate planet. The resulting new code (STOUR-AGA) formed the basis for a Master's thesis at Purdue by Bonfiglio.<sup>22</sup> This new program has been used to explore in detail the parametric trajectory space that exists for the AGA concept as a function of launch energy, waverider L/D ratio, and which intermediate planets will be chosen for a near optimum AGA trajectory to a destination.

Another teaming relationship has recently developed as a result of a new NASA initiative that has formed an Aeroassist Team composed of members from the NASA centers who are developing a future technology plan for aeroassist technologies, including the AGA technology. As a result of this initiative, a new group from NASA Ames Research Center (ARC) has been added to our AGA team. Members of this group bring to the team expertise in high temperature thermal protection systems (TPS) and materials, as well as an experience in flight testing of aerodynamic entry systems. The new materials that are under development as part of the SHARP program at ARC promise to perform well in the extreme TPS environment of AGA maneuvers.

This paper will include the latest results from the waverider configuration designs from Maryland, the parametric trajectory studies from Purdue, the TPS materials research at NASA ARC, and the atmospheric flight simulations that have been completed at JPL.

Figure 1 illustrates a planetary waverider: launched to HEO on a Delta II 7925 or carried to LEO on the Venture Star. In both cases the waverider would have a LH-LOX linear aerospike engine to produce a C<sub>3</sub> of over 50 km<sup>2</sup>/s<sup>2</sup>, entailing a delta-V of over 5.2 km/s from LEO and over 2.0 km/s beyond the Delta from HEO.

### WAVERIDER DESIGN

Waveriders are supersonic shapes in which the bow shockwave is directly attached to the leading edge. This means that all of the flow that passes through the shockwave on the lower lifting part of the waverider is contained below the waverider. This has the benefit of producing a generally high value of available lift/drag ratio (L/D) at high Mach numbers with high lift, and reducing cross flow and non-uniformities on the compression surface.

Waveriders were first defined by Nonweiler.<sup>3</sup> They are generated by starting with a known flow with a given shockwave; a stream surface parallel to the direction of flow under the wedge is selected to represent the lower surface of the waverider. The intersection of that lower surface and the original shockwave defines the leading edge with an attached shockwave. This whole process works because the flowfield is mathematically hyperbolic, so that the carved-out section which forms the waverider surface, representing perhaps a small portion of the original flowfield, still retains the properties of that flowfield even though the generating body has been ignored once the waverider is defined.

Other generating bodies can also be used as the starting point of the waverider flowfield design process. Conically-derived waveriders have been used extensively because they tend towards higher volumetric efficiency than the wedge-derived forms. Combinations of cones and wedges have also been explored for creating the generating flowfield.<sup>16</sup> For a given flight Mach number, both the wedge and cone-shaped forms have only one degree of freedom: the oblique surface angle. Burnett and Lewis<sup>17</sup> showed that conically-derived shapes can also be optimized with volumetric considerations, to produce vehicle forms that strike an acceptable compromise between aerodynamics and packaging, and with realistic, rounded leading edges. In fact, nearly any shape that has associated with it a shockwave and supersonic downstream flow can be used as the initial generating body for a waverider. In turn, each generating flowfield contains an infinite number of stream s

urfaces which can be selected to form the final waverider, so there is great flexibility in the process, which leads easily to the application of optimization.

Considerations other than simple aerodynamics and volume can be included in waverider optimization. For instance Tarpley and Lewis<sup>18</sup> showed the effects of steady state flight and static margin constraints on the optimized design for an engine-integrated wedge-derived waverider. The performance of the optimized vehicle, which included the steady state flight constraints, is significantly greater than the performance of the vehicle optimized with no steady state flight constraints assuming that control surface deflections must be included for trim.

Ideally, the design of an AGA vehicle, should be optimized for the entire trajectory, from atmospheric entry to exit back to space. For a multiple-pass AGA, which may involve flight at several different sustained Mach numbers in different planetary atmospheres, it is not even obvious which is the best design point to select. Although software and the hardware are available to accomplish this task, from a practical stand point it remains a challenge to implement.

In this study, an AGA vehicle had been designed using a so-called "osculating cone" waverider, with a flowfield constructed from numerous slices of conical flow. The waverider has been optimized to fit within a constrained volume, corresponding to a launch vehicle enclosure. The method of generating an osculating cone waverider is described below.

Given that hypersonic waveriders are generally designed using an inverse process in which a flow field is first selected around a chosen generating body, an intriguing question is: what is the "best" generating shape to use in forming that initial generating flow field? Since the waverider is generated only from a portion of the flow field, the characteristic of the generated waverider shape may not necessarily reflect the characteristic of the generating shape. In contrast, waverider shapes generated from axi-symmetric flow fields have better aerodynamic performance with greater volumetric efficiency; however, the flow coming off the forebody is no longer uniform, and for a given inlet width the mass capture area is smaller. Furthermore, an axi-symmetric forebody/inlet combination requires greater turning angles and contraction ratio for a given pressure rise, which can increase the cross-sectional area of the vehicle.

Hence, what is truly desired is a generating flow field that can generate a waverider shape with the positive attributes of the waveriders derived from the two generating flow fields. One option is to use a hybrid geometry for the generating shape. For instance, a hybrid cone-wedge shape has been used to successfully generate a waverider that has a uniform forebody flow, like a wedge-derived waverider, but with a good volumetric efficiency, like a conically-derived shape.<sup>16</sup> A flight test of a shape of this type is planned as part of the NASA Ames SHARP program. The hybrid shape introduces extra flexibility into the waverider optimization process by allowing the optimizer to expand or contract the dimension of the wedge segment relative to the cone, and therefore make the flow field more wedge-like or cone-like. However, since this method requires a three dimensional Euler calculation for each generating body, it is not particularly well suited for preliminary vehicle design study, which may require exploration of numerous different shapes. Most recently, work has concentrated on an even more promising technique which eliminates the need to choose a generating body and permits direct specification of the desired shock wave instead. This is the so-called osculating (Latin for "kissing") cones waverider method developed originally by Sobieczky and coupled to an optimizer by Takashima and Lewis.<sup>19</sup>

In the method of osculating cones, the generating flow is defined by a design Mach number, a bow shock angle, and a shock wave shape at the exit plane of the waverider; hence, the method does not require a generating body to be defined. The flow field behind the non-axisymmetric shock is determined by assuming "locally conical" flow in the normal planes along the shock curve. The "locally conical" flow is defined by an osculating slice of flowfield. The shock angle as well as the Mach number which define the "locally conical" flow are kept constant in each osculating plane to ensure a smooth continuous lower surface on the generated waverider shape. The vertex of the conical flow field in each plane is determined by the local radius of curvature and the shock angle. The shock curve is chosen so that the change in the radius of curvature is continuous along the curve, and a series of planes is used along the shock curve in the exit plane to fully define the flow field behind the bow shock.

Note that in the limit of infinite radius of curvature, the conical flow degenerates into a wedge flow, so that by prescribing a flat shock curve, a wedge caret-wing waverider can be generated with the osculating

cone method. Similarly, a conical waverider can be generated by simply prescribing a shock curve with constant radius of curvature, i.e., a circular arc. Thus, by choosing a shock curve which has an infinite radius of curvature along the center region and a finite radius of curvature along the outboard region, the two positive attributes of the two generating flow fields, a wedge flow and a conical flow, can be combined in a single waverider. Since the flow field is assumed to be locally axisymmetric, the method can be inaccurate when large spanwise pressure gradients are present; however, such a flow would have a corresponding shape with large surface curvature, which would likely not be suitable for practical applications. Moreover, the integrated aerodynamic forces calculated by the method matched well with the values calculated numerically. More importantly, the flexibility provided by the technique has already been shown to produce shapes with superior aerodynamic and volumetric performance compared to the simpler wedge- and cone-derived forms, and the greater flexibility also enables the designer to place a waverider aerodynamic shell around an existing vehicle with specified geometry and volume.

Once the generating flow field is established, an osculating cone waverider shape is determined by selecting a leading edge at the exit plane, subject to certain limits of permissible geometry. When the vertex of the osculating cone and the leading edge point is determined, the lower surface of the waverider can be constructed by tracing the streamline along a known conical flow, analogous to the generation of a conical waverider. If the shock curve is flat, i.e., the radius of curvature is infinite, the slope of the streamline will be a constant value which is equal to the wedge angle which produces the given bow shock angle for the given design Mach number.

One of the most important characteristics of the waverider design is that it is an inverse process, where a desired flow field is first selected and then a shape which produces the generated flow field is determined. For any given generating flow field, an infinite number of waveriders can be selected by varying the shock-intersection curve. For the osculating cone waverider design, the shock wave shape can also be varied. Thus, an optimizer can be used to select the "best" shape among many, where "best" is defined by some objective function that can relate either to the pure aerodynamic form or an integrated performance parameter. In this study, the sequential quadratic programming method as implemented by Design Optimization Tools (DOT) available through VMA

Engineering, is used to optimize the design for maximum cruise range performance.

The gradients used in the algorithm are calculated using finite differences by the optimization code. Even for a highly interdisciplinary design, the number of variables required to define a waverider are limited and the objective function is readily calculated by analytical means, so the cost of calculating the finite difference gradients is not severe.

Application of optimized waverider forms was described by Lewis and McDonald.<sup>12</sup> Figure 1 shows a representative waverider vehicle design. To accurately predict the surface flow properties, a hybrid method of tangent-wedge and tangent-cone methods is used. For the rest of the airframe, the surface properties are calculated using the shock-expansion method. The viscous forces on all the surfaces are calculated using a reference temperature method. The flow is assumed to be entirely turbulent with constant wall temperature.

The waverider in Figure 2(a) was optimized for maximum L/D, and to fit within a Venture-star-class payload bay. Maximum L/D is 8, and volume is 17 m<sup>3</sup>. Figure 2(a) shows this shape and Fig. 2(b) shows its aerodynamic performance ( $C_L$ ,  $C_d$ , L/D) as a function of the angle of attack  $\alpha$ , for turbulent boundary layer conditions. Figure 2(c) and Figure 2(d) show the same parameters for a laminar boundary layer. Note that below the design attitude, L/D falls off rapidly, but at large angles of attack (AOA), L/D is relatively insensitive.

#### AUTOMATED SEARCHES FOR AGA TRAJECTORIES

Using a constant L/D assumption, an AGA algorithm was developed that accounts for drag and was suitable for installation into a program known as STOUR (Satellite Tour Design Program). STOUR was originally developed<sup>14</sup> at JPL where it was used interactively to design the Galileo Orbiter Tour. The program was upgraded at Purdue to perform automated design for a variety of gravity-assist missions.<sup>20</sup> A detailed description of the AGA algorithm that was used in the latest version of the program known as STOUR-AGA can be found in Bonfiglio, Longuski, and Vinh.<sup>21,22</sup> Sims, Longuski, and Patel<sup>23</sup> and Bonfiglio<sup>22</sup> used an automated search method to determine AGA trajectories but assumed an infinite L/D ratio and later provided analytic approximations of drag effects.

There are many potential missions that could benefit from AGA trajectories. A Neptune orbiter might be very interesting, especially if AGA is able to reduce the launch energy and time of flight required. Currently, a number of missions are being planned to Mars. Cheaper free-return trajectories that can obtain atmospheric samples would provide valuable science. AGA sample-return missions from the atmosphere of the gas giants (such as Saturn) could be used to determine the age of these distant planets. The missions that were investigated use Venus and Mars for AGA. Randolph and McDonald<sup>11</sup> found the combination of Venus and Mars for AGA to be extremely beneficial, because of the lower launch energy to the first planet (Venus), and the lower periapse speed of the second planet (Mars).

One mission of great interest for the past few decades was a Pluto flyby. Pluto is the only planet that has not been visited by spacecraft. For this reason, a mission to Pluto is very exciting and scientifically important. The current reference mission to Pluto (now termed Pluto-Kuiper Express) uses an 8 year trajectory with a large launch vehicle (C3 about 150 km/s) and a gravity assist from Jupiter.<sup>24</sup> Figure 3 shows AGA results for a trajectory search with similar characteristics to the reference mission. Table 1 gives a legend for understanding the STOUR-AGA results. The assertion for our typical AGA trajectories is that both Venus and Mars AGA maneuvers are necessary. Thus the "path" of preference would be "3 2 4", followed by the final body as shown in Figure 3 (i.e., path 3249 goes to Pluto). A reasonable L/D ratio for the waverider development at this time would have a value less than 10, with a typical value of 7 at both Venus and Mars, as shown in Figure 3. With this L/D the parametric variable of Figure 3 is the launch hyperbolic excess velocity ( $V_{\infty}$ ) which should be minimized to enable small (inexpensive) launch vehicles to be used. Table 2 provides example data from two AGA trajectories for comparison against the 2004 reference mission.<sup>24</sup> In the first example, we see that if we use the exact same launch  $V_{\infty}$  for an AGA trajectory (12 km/s), then the time of flight is reduced by 3 years (compared to the 8-year time of flight of the baseline mission). But, of course, this implies a very large launch vehicle, which is not the goal of AGA. However, if we match the 8-year time of flight with an AGA, we can reduce the required launch  $V_{\infty}$  by about 4.5 km/s, which means that a smaller and cheaper class of launch vehicles could be used. We

conclude from these comparisons that AGA can provide an advantageous trade-off between time of flight and total launch energy.

Now that we have shown AGA to outperform pure gravity-assist missions in terms of launch  $V_{\infty}$  and time of flight, it is useful to determine the best AGA trajectories for various missions. (A more detailed search is provided in Bonfiglio, Longuski, and Vinh).<sup>21,22</sup> When designing a mission the definition of "best" can sometimes be ambiguous. The best AGA trajectories here have been determined on the basis of launch  $V_{\infty}$ , time of flight, and to a lesser extent arrival  $V$ . Table 3 gives a list of the most promising trajectories for the missions mentioned above. We see from this table that trajectories to Pluto and Neptune exist with times of flight less than 5.5 years, with an L/D of 10. Additionally, the Mars free-return trajectories give very promising results.

Patel, Longuski, and Sims<sup>25,26</sup> did extensive research on Mars free-return trajectories using a launch date range of 1/1/1995 to 1/1/2020. They showed that trajectories with a 2-year time of flight and a launch  $V_{\infty}$  of at least 6.0 km/s exist approximately every two years. They found trajectories with very fast times of flight (about 1.5 years), but with a higher launch  $V_{\infty}$  of 7.0 km/s, and high arrival  $V_{\infty}$  (between 8 km/s and 10 km/s). These trajectories do not occur often, existing only in 2000, 2002, 2015, and 2017 for their 25-year search. If a very low L/D ratio of 3 is used for the free-return path, shorter times of flight exist with even lower launch  $V_{\infty}$  values. An independent re-creation of the Patel, Longuski, and Sims fast trajectories (with STOUR-AGA), shows the arrival dates are identical to the arrival dates for the Mars AGA trajectories with times of flight of 1.0 year. This comparison supports the notion that the best AGA trajectories are the trajectories found by Patel, Longuski, and Sims, but are improved by AGA (reducing launch  $V_{\infty}$  as much as 4.5 km/s). The arrival  $V_{\infty}$  for the Mars AGA trajectories is still high, but is alleviated by using the VM path for the free return. Using the VM path, a time of flight of 1.3 years can be obtained with a launch  $V_{\infty}$  of 4.0 km/s with much lower arrival  $V_{\infty}$ s (e.g. 3 km/s vs 9 km/s) compared to the best time of flight case for a pure gravity assist (using ME).

Finally, the Saturn free-return trajectories provide short flight times and low launch  $V_{\infty}$  values. The arrival  $V_{\infty}$  values at Earth are fairly high, but the ability of the waverider to perform aerocapture upon return to the Earth alleviates this problem.

Table 1

## Legend for STOUR-AGA Launch-Date Plots

PATH	Planets encountered, including launch and destination bodies, e.g. PATH: 3 5 9 uses a Jupiter gravity assist from Earth to Pluto
v <sub>inf</sub>	Launch V <sub>∞s</sub> . The numerals 1, 2, 3, 4,...on the plot represent the 1 <sup>st</sup> , 2 <sup>nd</sup> , 3 <sup>rd</sup> , 4 <sup>th</sup> , ... V <sub>∞s</sub> in the list. If an AGA maneuver is used during the trajectory then, A,B,C,D,... is used instead of 1,2,3,4,... . E.g. in Figure 3 the 'D' on the plot denotes a V <sub>∞s</sub> of 12 km/s. For an STOUR-AGA plot, it is possible to have both AGA and pure gravity assist points on each plot.
Lift/Drag	Lift/Drag ratio used at each AGA planet. If Lift/Drag=0 then there was no AGA performed at that planet. E.g. in Figure 3 the Path=3 2 4 9 and the Lift/Drag=0.0 .0 7.0 0.0 means there is no AGA maneuver at the first and last planet in the path, but AGAs with Lift/Drag=7 are possible at the 2nd and 3rd planet in the path.
Search Event	Event Path for which data are plotted. E.g. in Figure 3, TOF to Pilluto is plotted since encounter with Pluto is the 4 <sup>th</sup> event in the PATH.
ALTMIN	Minimum flyby altitude permitted in the STOUR-AGA run.
Search Min	Trajectories with flyby altitudes below this value are not included in the plot
Launch Dates Searched	Launch-date range (YYMMDD) used in the STOUR-AGA run. E.G. 05/01/01 means January 1, 2005. The launch-date increment is also given, for example "by 15 days.
TFMAX	Maximum allowable time of flight plotted.

Table 2

## Pluto Trajectory Comparisons

Reference Mission		Comparable AGA Trajectories		
Time of Flight (years)	Launch V <sub>∞s</sub> (km/s)	Time of Flight (years)	Lift/Drag Ratio	Launch V <sub>∞s</sub> (km/s)
8.0	12.0	5.0	7	12.0
		8.0	7	7.45

Table 3.

## AGA Trajectories for Various Missions

Path	Launch Date (MM/DD/YY)	TOF (years)		Launch $V_\infty$ (km/s)	Arrival $V_\infty$ (km/s)	Lift/Drag Ratio
Pluto						
VM	10/31/13	5.2		9.0	30.5	10
VM	10/16/13	6.7		8.0	22.8	7
VM	10/16/13	7.2		9.0	21.1	5
Neptune						
VM	3/27/06	5.4		7.0	28.2	70
VM	3/27/06	6.2		7.0	24.1	7
VM	3/27/06	7.7		7.0	18.2	5
Mars Free-Return						
VM <sup>a</sup>	8/18/02	1.3		4.0	3.1	1
M	3/28/14	2.4		3.5	4.5	5
Saturn Free-Return						
VMS	5/21/07	5.3		5.5	12.5	10
VMS	5/21/07	6.4		5.5	19.7	7
VMS	5/21/07	6.4		6.0	22.2	5

<sup>a</sup> The only AGA is at Mars in this trajectory.

ATMOSPHERIC FLIGHT PARAMETERS

Figure 4 (a and b) illustrates the rotation of the Vinf vector that changes the heliocentric vector that is inherent in AGA. This section gives some example parameters for AGA flight in the atmospheres of Venus and Mars. Since the heliocentric velocity gain from AGA increases with the size of the Vinf vector it is appropriate to consider substantial Earth Vinf values, such as 7 km/s ( $C3 = 49 \text{ km}^2/\text{s}^2$ ). Figure 4(c) illustrates typical AGA trajectory outcomes using Mars as the intermediate planet. A retrograde flyby allows a return to the inner solar system (e.g. earth), whereas, a direct flyby heads for the outer solar system. Typical AGA parameters for AGA at Venus and Mars are shown in Fig. 5 (from Ref. <sup>9</sup>): (a) velocity, (b) bending angle, (c) atmospheric flight time, and (d) travel time, as a function of Earth launch velocity, VinfE. The line at VinfE = 7 km/s on Fig. 5 (a) indicates that VinfV would be about 15 km/s, that Vp (the periapsis speed) at Venus would be about 18 km/s, while at Mars the corresponding values would be about 25 km/s, assuming no drag loss at Venus. It will be shown below that the drag loss at Venus is about 3.5 km/s, and  $L/D = 5$ , and one should adjust the VinfE accordingly to find V at Mars.

FLIGHT ALTITUDE

The flight altitude for AGA and the velocity loss due to drag can be evaluated from two equations:

$$\frac{1}{2} \rho V^2 C_L \frac{A}{m} = \frac{V^2}{R} - g \quad (1)$$

$$\Delta V_\infty / V_\infty = \frac{-\phi}{\left(\frac{L}{D}\right)} \left[ 1 + \left( \frac{V_c}{V_\infty} \right)^2 \right] \quad (2)$$

where  $V_c$  is the circular velocity,  $\rho$  is the atmospheric density  $V_\infty$  is the velocity at infinity.

Figure 6 shows (a) the value of  $BL = m/CdA$ , where  $CL$  is the aerodynamic lift coefficient,  $m$  is the mass, assumed for now to be 1000 kg,  $A$  is the planform area, taken as 114 m<sup>2</sup>, and  $Cd$  is the drag coefficient, and (b)  $CL/Cd$  ( $L/D$ ) as a function of angle of attack,  $\alpha$ . One can see that the AGA flight should stay within the range about 1 to 5 deg of  $\alpha$  to maintain near maximum  $L/D$ .

Figure 7 shows the equilibrium, atmospheric density in AGA, on the left hand scale, as a function of  $BL = m/CLA$  on the top scale, shown by the solid lines for Venus and Mars. The assumed values of  $m$  and  $A$  are  $m = 1000 \text{ kg}$ , and  $A = 114 \text{ m}^2$ , so that  $CL$  follows from a given value of  $BL$ . The scales of AOA  $\alpha$  at the bottom are the values from Fig. 2(b) (turbulent) and Fig. 2(d) (laminar) corresponding to  $BL$  across the top. Within the figure vertical lines from the AOA scales map out a region of density for

level flight at Venus and Mars with level speeds of 12, 14, 16 and 18 km/s. The horizontal lines going to the density scale span the region for AOA 1 to 5 deg (lift downwards) for the laminar boundary layer case. To the left of Fig. 7 there are scales showing the altitude at Venus and Mars corresponding to the density (Ref.<sup>27, 28</sup>). For example, the altitude range for Venus corresponding to AOA 1 to 5 deg and  $V = 12$  to 18 km is about 107 to 102 km, and for Mars it is about 59 to 51 km. The bottom scale on Fig. 7 is stagnation point heating rate, and the diagonal dashed lines marked "heating" show the convective heating rate,  $q_{ref}$ ,<sup>29,30, 31</sup>) to a cylinder of radius 0.3 m. It is well known that  $q_{ref}$  varies as the inverse square root of the nose radius ( $R_n$ ), and that the heating to a cylinder is less by square root of 2 than for a sphere of the same radius. The figure has a vertical line at 370 W/cm<sup>2</sup>, the flux that a body at 3000 K could radiate with emissivity 0.8 (a typical infrared value). The point shown on the line as a circle is a radiative flux calculated for  $R_n = 0.1$  m,  $V = 18$  km/s, and the density shown. At high speed the radiative heating is expected to exceed the convective. At a flux below 370 W/cm<sup>2</sup> a high-temperature radiator (described below) would not ablate, and above this temperature there would be ablation. If ablation is expected one might make the leading edge of carbon-phenolic, used on the Galileo probe,<sup>32</sup> which is a charring ablator capable of accepting much higher heating rates. In the Galileo case the predicted peak radiative flux to the probe nose was over 40 kW/cm<sup>2</sup> for a few seconds, and a longer convective heating pulse peaking at over 17 kW/cm<sup>2</sup>. The total time-integral was about 700 kJ/cm<sup>2</sup>, causing ablation of an estimated 2 inches of material, and to reach this value for Venus AGA, of duration about 500 sec, the heat flux would be 1.4 kW/cm<sup>2</sup>. Also, the thickness of leading edge material could be several inches, so that both the local flux and the time integral from the Galileo probe were considerably above the AGA requirements. Presumably a different waverider shape would be called for with a charring ablator. Also, one must consider the thickness of high-temperature thermal insulator necessary to keep the interior of the vehicle within bounds during a flight of 500 sec at Venus, and 200 sec at Mars.

From Eq. (2) for Venus and a  $V_{inf}$  at entry of 15 km/s, we can evaluate delta V to be about 3.5 km/s, i.e., the  $V_{inf}$  at exit will be about 11.5 km/s, and the  $V_{inf}$  at Mars will be reduced in accordance with the data of Fig. 5.

## LAUNCH CONFIGURATIONS

For launch and flight computations a mass of 1000 kg has been taken as nominal. For a vehicle of length 60 ft, (18.3 m), width 15 ft (4.57 m) and height 10 ft (3.05 m) (fits in the STS cargo bay) the surface area is about 114 m<sup>2</sup> for each of two surfaces. Taking a carbon-carbon material (specific gravity 2.4) of thickness 1 mm would give a mass of 550 kg. The launch to LEO could be on the STS or a vehicle like the Venture Star, as shown in Fig. 1 (b). To achieve a C3 of 49 km<sup>2</sup>/s<sup>2</sup> would require a delta V of about 5.3 km/s, requiring an initial mass (with LOX-LH propellant at Isp = 440 sec) of 3380 kg to deliver 1000 kg. Therefore the tanks and nozzle for the assumed linear aerospike type engine would have a mass of perhaps 240 kg. An alternative launch with a Delta II (see Fig. 1(a)) from HEO (C3 = -2 km<sup>2</sup>/s<sup>2</sup>) would require about 2.0 km/s, giving 1630 kg initial mass to deliver 1000kg, and perhaps 160 kg of tanks and nozzle. To give a worthwhile payload and the necessary avionics for the AGA flights, thermal protection, etc., would evidently require more than 1000 kg, but this value suffices to illustrate the design process.

## CONTROL

To fly at high speed in a corridor of a few km in altitude calls for rapid determination of the ambient aero lift acceleration force, and quick implementation of a pitch correction maneuver. The obvious method of control is a control surface at the rear (where the linear aerospike engine takes some of the space), which would change the effective AOA a degree or so by moving only a small amount (e.g., 10 % of the chord moving through 5 deg, probably using ram-air-derived power. We note that the aero heating on the wetted (top surface in AGA inverted flight) will be a few percent of the stagnation level, and the heating rate on the other surface will be even less. A rudder or wing-tip surfaces may be appropriate for yaw control. Control will be facilitated if the center of gravity (CG) can be kept well forward of the center of pressure (CP), which is expected to be at the centroid of area. Having engine nozzles along the rear brings the cg back, but the substantial leading edge thermal protection mass would bring it forward.

## ENTRY and EXIT

Some entry data are given in Table 4, showing entry angles for various constant L/D entry paths giving



level flight close to the equilibrium conditions. It should be noted that entry and exit occupy a certain angular range, and that a certain entry angle error or uncertainty will be present but significant corrections are possible by maneuvering in the atmosphere. The most likely entry configuration is inverted with downward lift at about a mid value, but one must consider that there is more lift available if the vehicle goes initially below the equilibrium altitude. The exit point should be adaptable in terms of the measured drag acceleration and its time integral, to come out with the highest V at an angular range of

the pass that will be targeted to the next planet. Figure 8 illustrates how travel time from Venus to Mars varies with V and exit angle (a), and how angular range from Venus to Mars varies with V and exit angle(b). From data of this type an adaptive algorithm would be on-board for AGA at Venus, to determine where to exit from the measured drag, to reach Mars with the shortest travel time and the least delta V correction, given the ambient losses in the Venus AGA.

Table 4. Some Venus entry cases close to desired level flight (102 to 107 km altitude); constant m/CdA, L/D assumed from entry to level-off

Level-off Altitude, km	Entry Speed, km/s	m/CdA, kg/m <sup>2</sup>	L/D	Entry angle, deg At Z = 125 km	Angular range from entry, deg
102.3	12	500	0	4.0	6.2
106.9	12	500	0	3.5	
102.0	12	500	+3	4.2	
105.7	12	200	+3	4.0	5.1.
106.8	12	200	+5	4.0	4.7
102.2	14	500	0	4.2	4.7
107.0	14	500	0	3.7	
105.9	14	500	+3	4.0	
108.5	14	500	-3	3.5	
107.8	14	500	-5	3.5	
102.0	16	500	0	4.5	4.0
107.2	16	500	0	3.7	
103.4	16	500	+3	4.5	
103.8	16	500	-3	4.0	
102.3	18	500	0	4.5	
107.0	18	500	0	4.0	4.7
104.1	18	500	+3	4.5	
105.5	18	200	+3	4.5	
106.5	18	200	+5	4.5	

#### TECHNOLOGY DEVELOPMENT NEEDS

An enabling technology for aero-gravity assist vehicles is the ultra-high temperature ceramic (UHTC) materials under development at NASA Ames. UHTCs have a unique combination of mechanical, thermal, and chemical properties that enable the fabrication of very small radius or sharp leading edges for non-ablating hypersonic operation. One of the most useful approaches for understanding the conditions where these leading edges are capable of operating without ablation is the aerothermal performance constraint (APC). APCs are determined

by numerical simulation of the coupled aerothermal heating / thermal response behavior of the UHTC leading edge to define the steady-state "non-ablating performance" constraint on the altitude-velocity flight envelope.<sup>33</sup> An APC for the 0.141 inch radius UHTC nosetip tested in the SHARP-B1 flight demonstration is shown in Fig. 9 along with a typical space shuttle orbiter trajectory.<sup>34</sup> By comparing a trajectory to an APC in this manner a vehicle designer can quickly determine if the vehicle will experience leading edge ablation. In this case no ablation occurs because the trajectory does not cross the APC.

At high altitude the APC becomes nearly parallel to the velocity axis (as shown by the dashed extrapolation line) because the transition from the continuum to the rarefied flow regime gradually reduces the aerothermal heating.<sup>35</sup> Figure 9 shows typical AGA flight profiles for Venus and Mars, at equivalent Earth altitude, indicating that there is some crossing of the APC. Aero-gravity assist trajectories that cross the APC cause ablation of the sharp UHTC leading edge introducing significant uncertainty into estimates of thermal protection system (TPS) performance, vehicle aerodynamics, and control capability. Trajectories that do not cross the APC minimize these uncertainties and simplify the vehicle design process. By utilizing APCs in this manner a vehicle designer would be able to quickly determine if the current vehicle design will experience leading edge ablation without waiting for an extensive thermal analysis. Simplifying the design process is important when attempting to rapidly move forward from concepts to actual flight hardware. Tests such as in the SHARP program will help to further understand and calibrate the APC analyses and the application to the leading edges of the AGA waverider vehicles.

Other technology development needs include control surface design, control computational design and software, and avionics hardware development. A program will be necessary to develop and fly test models of hypersonic waveriders subjected to environments similar to the AGA maneuvers at the planets. Such a program is in the planning stage by the AGA team represented in this paper.

### CONCLUSIONS

In general, AGA enhances the gravity-assist technique tremendously by reducing launch energy and decreasing flight time. This enhancement depends on the availability of high lift-to-drag hypersonic vehicles, as exemplified by current literature on the waverider. The results demonstrate that AGA is an enabling technology that can significantly reduce mission costs, increase science return, and allow greater access to the Solar System.

From this approximate analysis one can conclude that a vehicle with a mass about 10-15 kg/m<sup>2</sup> of plan area can be designed to fly AGA at Venus and Mars, beginning at Earth with a C3 of up to 50 km<sup>2</sup>/s<sup>2</sup>. There is a limiting speed  $V$  in AGA at Venus and

Mars where a sharp leading edge will begin to ablate, and beyond which the waverider design should include a degree of blowing, gas injected at the leading edge and lifting the boundary layer downstream to simulate ablation. For the ablating leading edge case the upper limit to the AGA speed, if a chine-type leading edge ablator is used, seems to be considerably above the value of  $V = 18$  km/s computed here.

It is clear that rapid small changes in vehicle angle of attack are needed, responding to measured lift accelerations, and analyses and tests are required to provide the necessary vehicle design parameters such as control surface area and location, center of gravity position, and pitch and yaw stability. Heating is a major parameter but being confined mainly to the leading edge it can be dealt with.

### RECOMMENDATIONS

1. System studies in more detail are required for several candidate missions. Two main classes of such missions are (1) atmospheric sample return from Mars with AGA at Mars, for isotopic analysis, and the same for Venus and other planets, including several planets on one flight; and (2) transportation type flights to Mars and other planets, delivering an orbiter or lander via a ballute, performing AGA to return to Earth orbit for the next payload.
2. Studies of rapid vehicle lift control in AGA, and development of an adaptive exit algorithm from measured drag and the estimation of the computational performance that will be necessary on-board to execute the algorithm.
3. Waverider designs including leading edge blowing, and appropriate wind tunnel simulations.
4. Earth entry waverider tests from secondary payloads on Delta or Ariane vehicles, entering at steep angles to give strong heating and ablation, and verification of aero characteristics.
5. A development program for ultra-high temperature non-ablating materials, charring ablator and low-density high temperature insulating materials should be actively pursued.

## REFERENCES

1. Randolph, J. E., Aero-Gravity-Assist Trajectory Analysis for Starprobe, JPL Internal IOM 312/82.5-981, 5 August 1982
2. Longuski, J. M., Can Aero-Gravity-Assist through the Venusian Atmosphere Permit a Near Radial Trajectory into the Sun, JPL EM 312/82-133, December 1982
3. Nonweiler, T. R. F., Aerodynamic Problems of Manned Space Vehicles, Journal of the Royal Aeronautics Society, Vol. 63, September 1959, pp. 521-528
4. Bowcutt, K. G., Anderson, J. D., and Capriotti, D., Viscous Optimized Hypersonic Waveriders, AIAA Paper No. 87-0272, 12 January 1987
5. Anderson, J. D., Jr., A Survey of Modern Research in Hypersonic Aerodynamics, AIAA Paper No. 84-1578, 25 June 1984
6. Randolph, J. E., McDonald, A. D., Solar Probe Mission Status, AAS Paper 89-212, 24 April 1989
7. Lewis, M. J., Kathari, A. P., The Use of Hypersonic Waveriders for Planetary Exploration, presented at the AIAA/JPL 2nd International Conference on Solar System Exploration, 22 August 1989
8. Lewis, M. J., The Use of Hypersonic Waveriders for Aero-Assisted Orbital Maneuvering, Proceeding of the 30th International Conference on Aviation and Space, February 1990
9. McDonald, A. D., Randolph, J. E., Applications of Aero-Gravity-Assist to High Energy Solar System Missions, AIAA Paper No. 90-2891, 20 August 1990
10. McDonald, A. D., Randolph, J. E., Hypersonic Maneuvering to Provide Planetary Gravity Assist, AIAA Paper No. 90-0539, 8 January 1990
11. Randolph, J. E., McDonald, A. D., Solar System Fast Mission Trajectories Using Aero-Gravity-Assist, AIAA Paper No. 91-0531, 7 January 1991, and J. Spacecraft and Rockets, Vol. 29, No. 2, pp. 223-232, March-April, 1992.
12. Lewis, M. J., McDonald, A. D., Design of Hypersonic Waveriders for Aeroassisted Interplanetary Trajectories, AIAA Paper No. 91-0053, 7 January 1991
13. Gillum, M., Kammeyer, M., Burnett, D., Wind Tunnel Results for a Mach 14 Waverider, AIAA Paper No. 94-0384, 10 January 1994
14. Williams, S. N., Automated Design of Multiple Encounter Gravity-Assist Trajectories, Masters thesis, Purdue University, August 1990
15. Takashima, N., and Lewis, M.J., "A Cone-Wedge Waverider Configuration for Engine-Airframe Integration," AIAA Journal of Aircraft, Vol. 32, No. 5, pp. 1142-1144, Sept-Oct. 1995.
16. Burnett, D., and Lewis, M.J., "A Reevaluation of the Waverider Design Process," AIAA 93-0404 presented at AIAA Aerospace Sciences Meeting, Reno, Nev., Jan. 1993.
17. Tarpley, C., and Lewis, M.J., "Stability and Control of Hypersonic Waverider Vehicles," AIAA Journal of Aircraft, Vol. 32, No. 4, pp. 795-803, July-August 1995.
18. Takashima, N., and Lewis, M. J. "Optimization of Waverider-Based Cruise Vehicles with Off-Design Considerations," AIAA Journal of Aircraft, Vol. 36, No. 1, Jan-Feb 1999, pp. 235-245.
19. J.M. Longuski and S.N. Williams, "Automated Design of Gravity-Assist Trajectories to Mars and the Outer Planets," Celestial Mechanics and Dynamical Astronomy, Vol. 52, No. 3 pp. 207-220, 1991.
20. E.P. Bonfiglio, J.M. Longuski, and N.X. Vinh, "Automated Design of Aerogravity-Assist Trajectories," AAS 99-361, Anchorage Alaska, August 1999, AAS/AIAA Astrodynamics Specialist Conference.

22. E.P. Bonfiglio, "Automated Design of Gravity-Assist and Aerogravity-Assist Trajectories," Master's Thesis, School of Aeronautics and Astronautics, Purdue University, West Lafayette IN, August 1999.
23. J.A. Sims, J.M. Longuski, and M.R. Patel, "Aerogravity-Assist Trajectories to the Outer Planets and the Effect of Drag," To Appear in Journal of Spacecraft and Rockets.
24. J.M. Ludwinski, "Pluto-Kuiper Express Preliminary Mission Plan," Jet Propulsion Laboratory, JPL Publication, Pasadena CA, December 1998.
25. M.R. Patel, "Automated Design of Delta-V Gravity-Assist Trajectories for Solar System Exploration," Master's Thesis, School of Aeronautics and Astronautics, Purdue University, West Lafayette IN, August 1993.
26. M.R. Patel, J.M. Longuski, and J.A. Sims, "Mars Free Return Trajectories," Journal of Spacecraft and Rockets, Vol. 35, No. 3, pp. 350-354, May-June 1998.
27. (Ed.) A. Kliore, The Venus International Reference Atmosphere, Advances in Space Research, Vol. 5, No. 11, Pergamon Press, 1985.
28. (Ed. ) A. Kliore, The Mars Reference Atmosphere, Advances in Space Research, Vol. 2, No. 2, Pergamon Press, 1982.
29. L. L. Perini, Compilation and Correlation of Stagnation Convective Heating Rates on Spherical Bodies, J. Spacecraft & Rockets, Vol. 12, March, 1975.
30. W.A. Page and H.T. Woodward, Radiative and Convective Heating During Venus Entry, AIAA J., Vol. 10, No. 10, 1379-81, October, 1972.
31. K. Sutton and R. A. Graves, "A general Stagnation Point Convective Heating Equation for Arbitrary Gas Mixtures" NASA TR R-376, November 1971.
32. J.N. Moss and E.C. Anderson, Aerothermal Environment for Jupiter Entry Probes, ? 1976.
33. P. Kolodziej, J.D. Bull, F.S. Milos and T.H. Squire, Aerothermal Performance Constraints for Small Leading Edges Operating at Hypervelocity, NASA CP-3359, 91-98, Sept. 1997.
34. P. Kolodziej, J. Bull, J. Salute, and D.L. Keese, First Flight Demonstration of a Sharp Ultra-High Temperature Ceramic Nostetip, NASA TM-112215, Dec. 1997.
35. P. Kolodziej, Aerothermal Performance Constraints for Hypervelocity Small Radius Unswept Leading Edges and Nostetips, NASA TM 112204, July 1997.

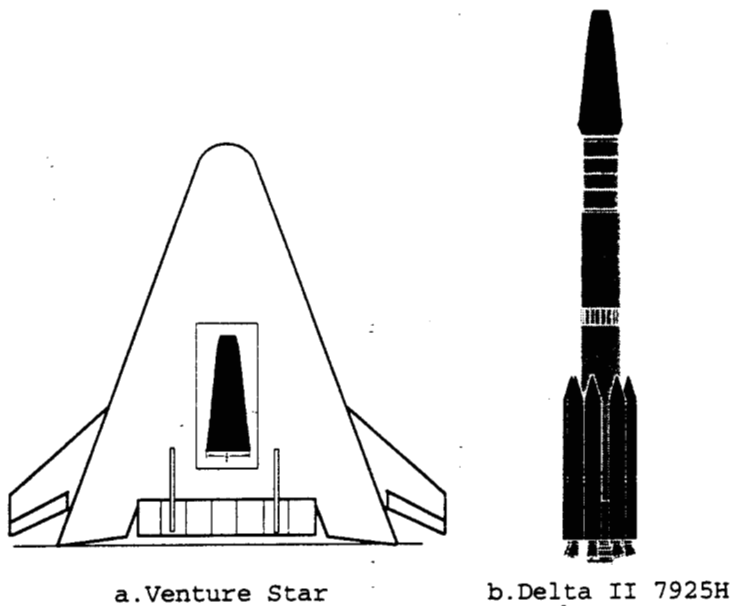
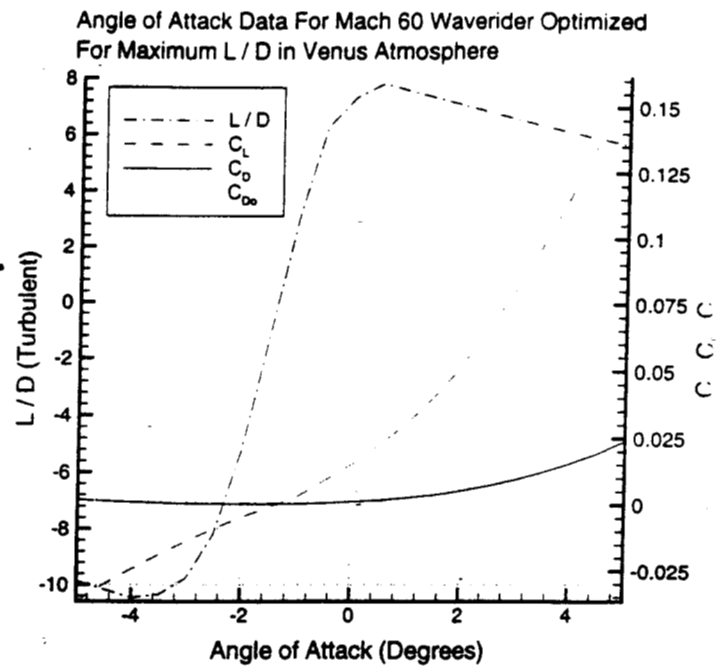


Fig. 1. Illustration of waverider : (a) carried to LEO on the Venture Star; (b) carried to LEO on the Delta II 7925H



2(b) aerodynamic performance, turbulent boundary layer;

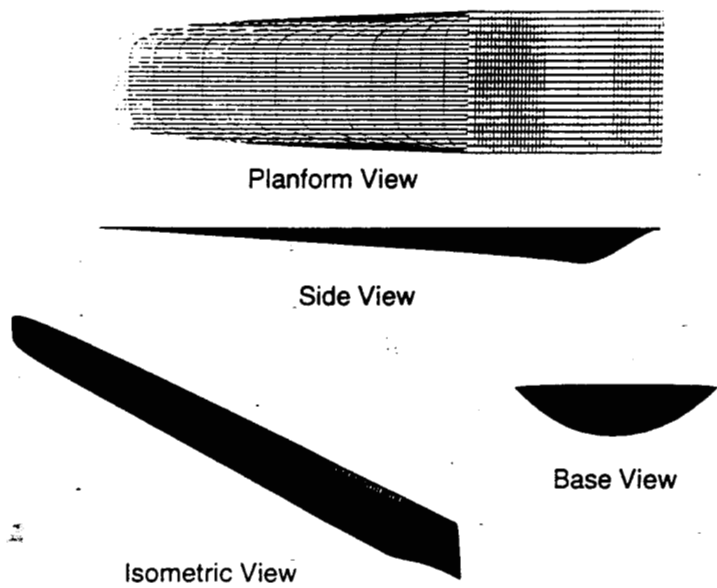
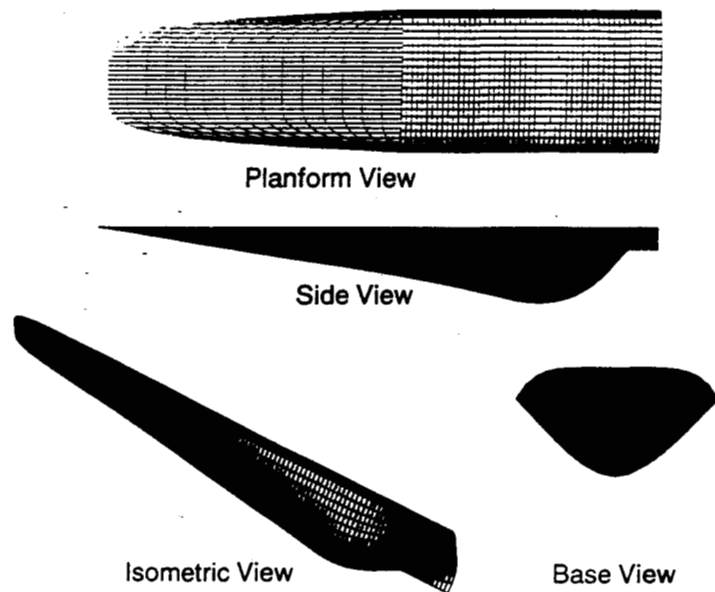
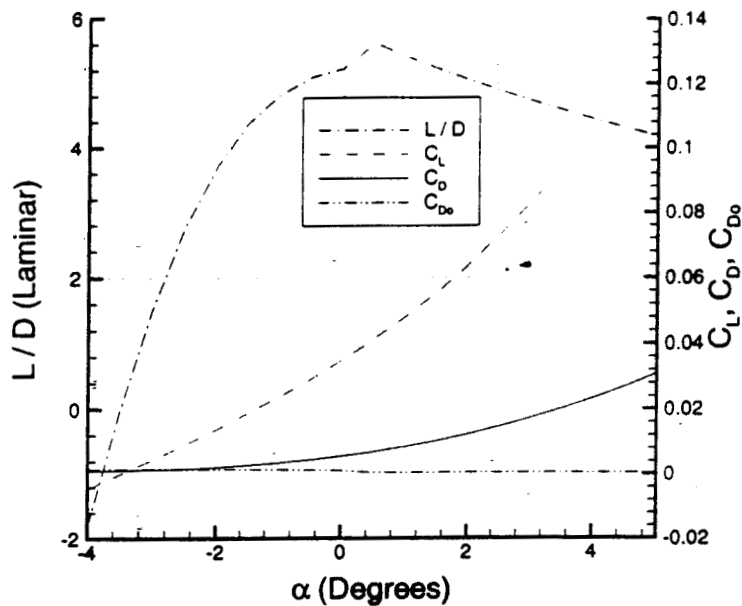


Fig. 2. (a) Waverider shape for a turbulent boundary layer

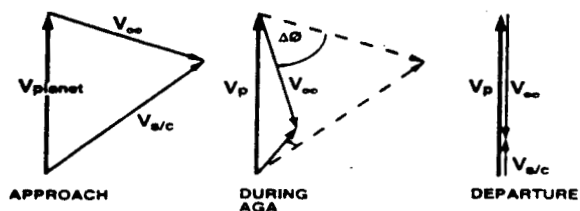


2(c) shape for laminar boundary layer;



2(d) Aerodynamic performance for a laminar boundary layer

#### a. DECREASE VELOCITY (e.g. SOLAR PROBE)



#### b. INCREASE VELOCITY (e.g. OUTER PLANETS MISSION)

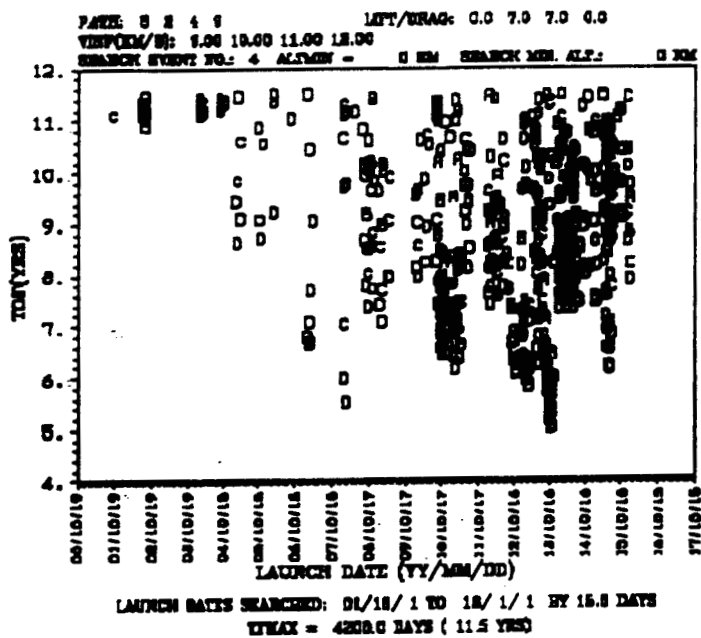
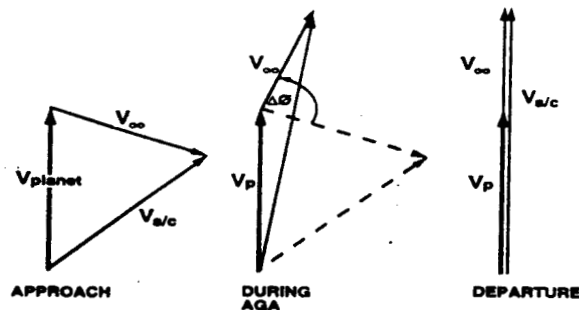


Fig. 3. Travel times for Pluto opportunities with AGA at Venus and Mars.

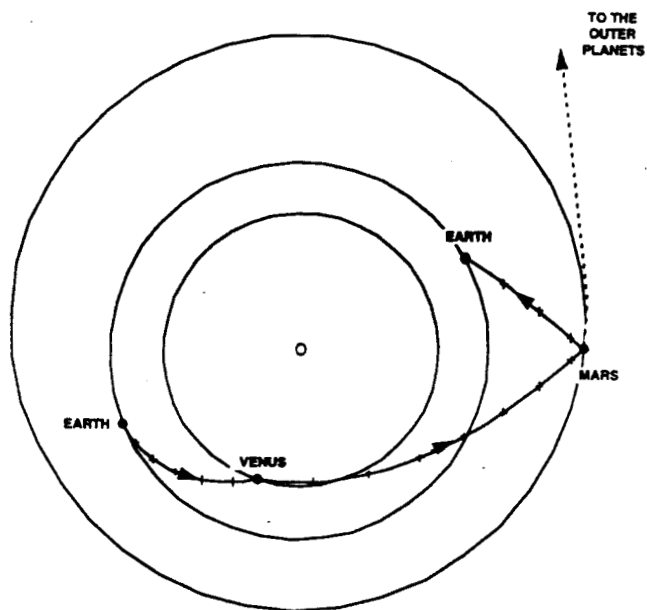


Fig. 4. Illustration of AGA: rotation and decrease of the  $V_{\infty}$  vector, and trajectory options

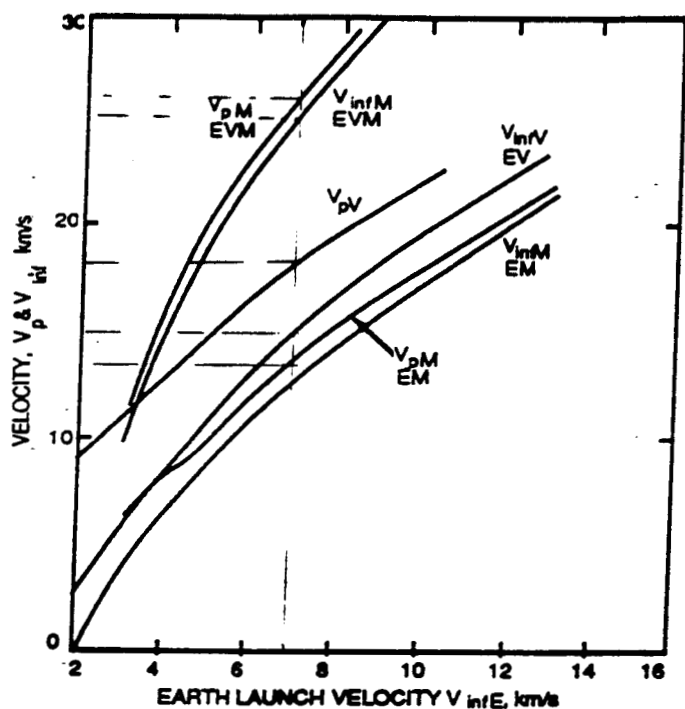
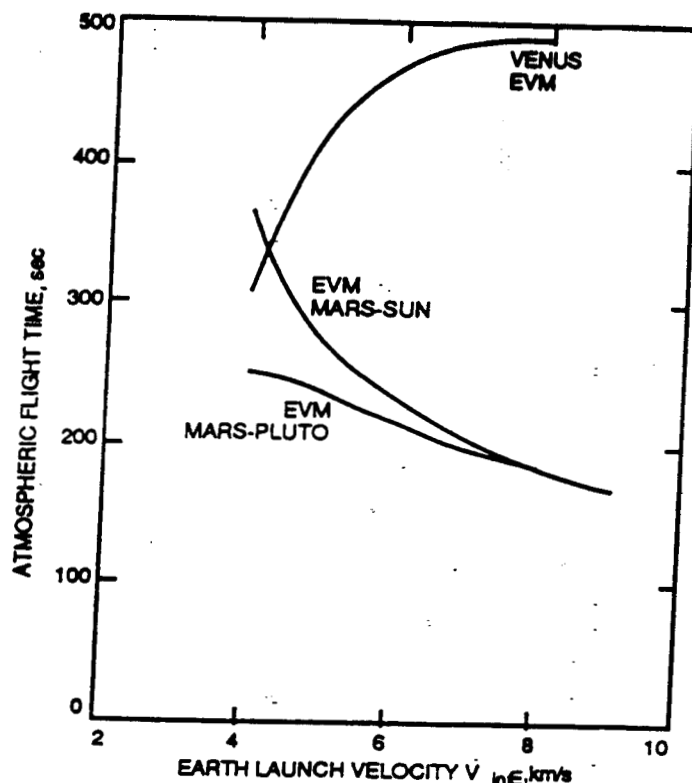
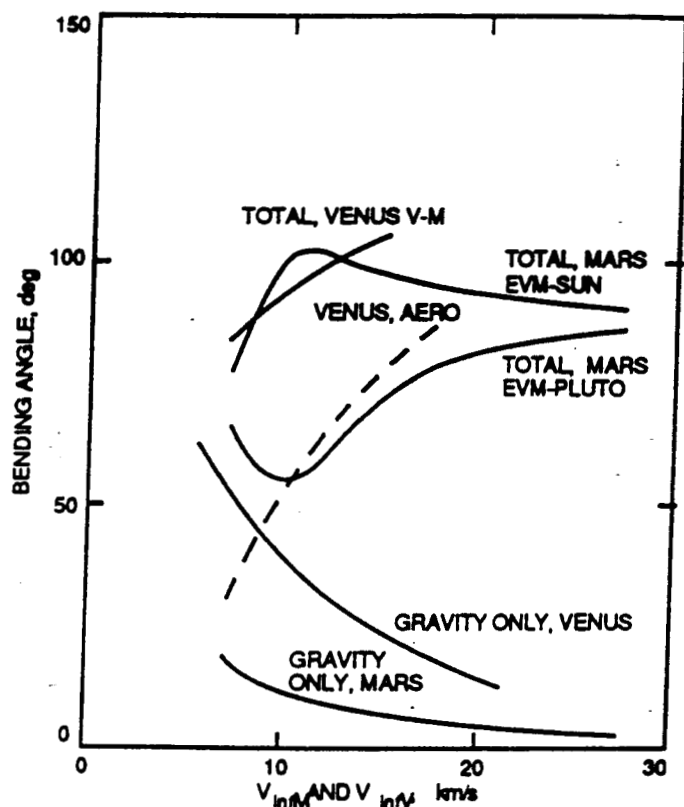


Fig. 5. Approximate parameters for AGA at Venus and Mars as a function of  $V_{inE}$  at Earth:

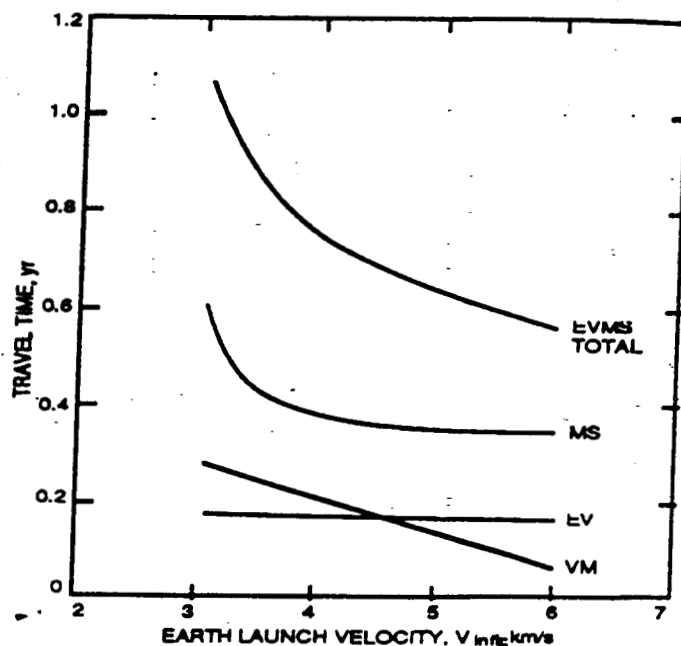
5(a) Planet velocities



5(c) Atmospheric flight time



5(b) Turn angles



5(d) Interplanetary travel times

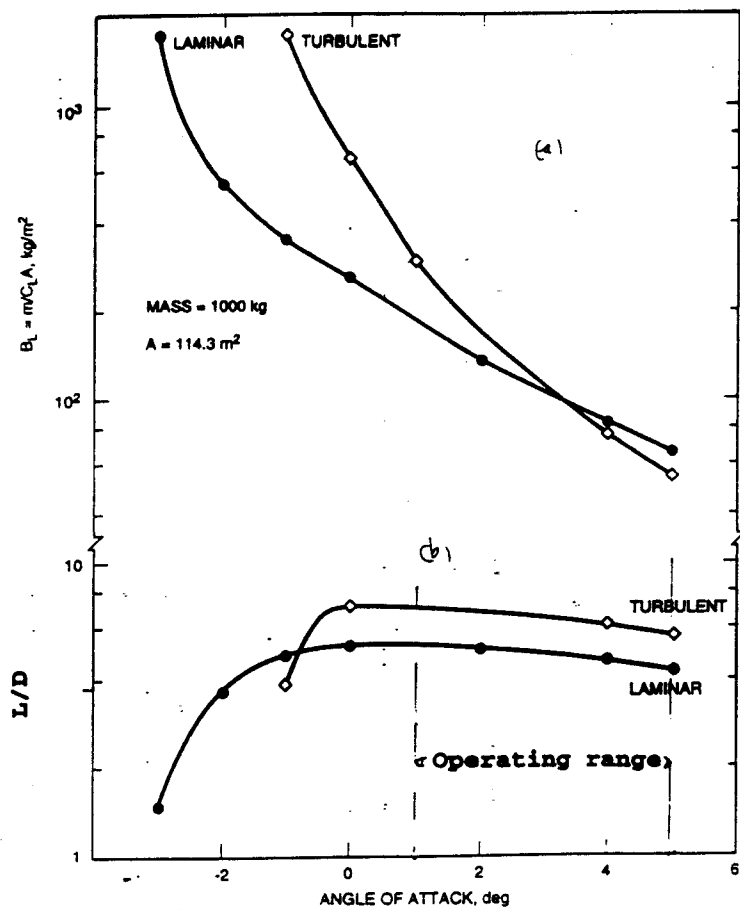


Fig. 6. (a)  $BL = m/CLA$  and (b)  $L/D$  as a function of angle of attack (AOA).

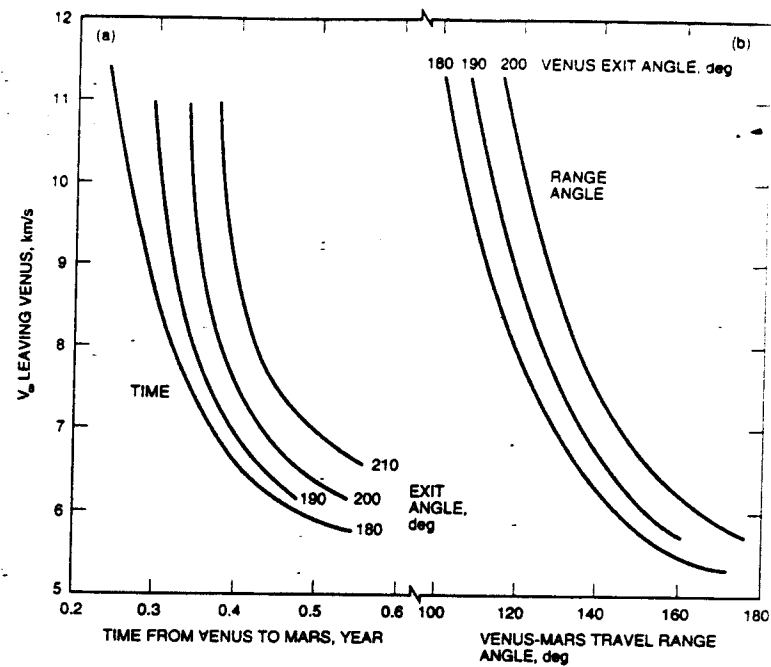


Fig. 8. Venus-Mars travel time (a) and travel range angle (b) as a function of  $V_{in}/V$  for different exit angles at Venus.

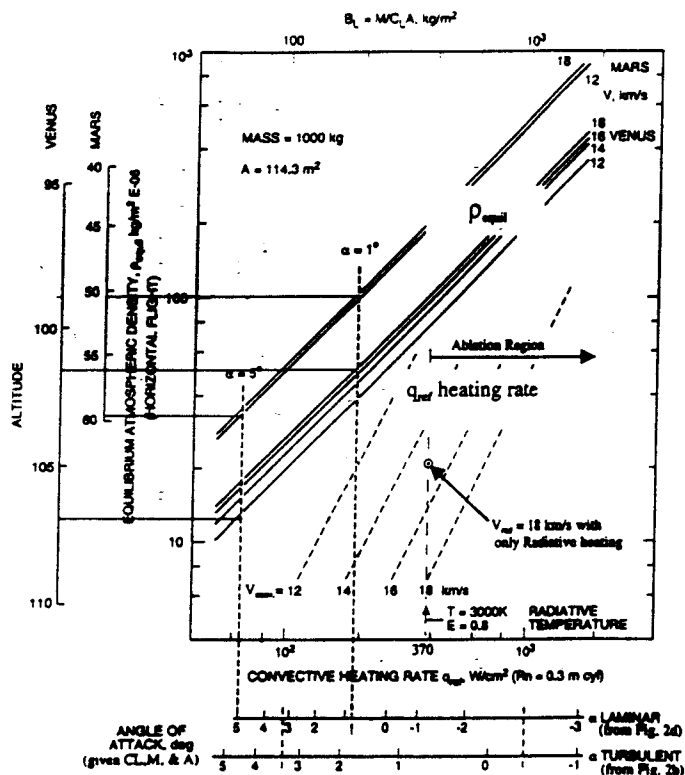


Fig. 7. Equilibrium AGA atmospheric density and convective heating rate as a function of  $BL = m/CLA$  for  $V = 12$  to  $18$  km/s in AGA at Venus and Mars.

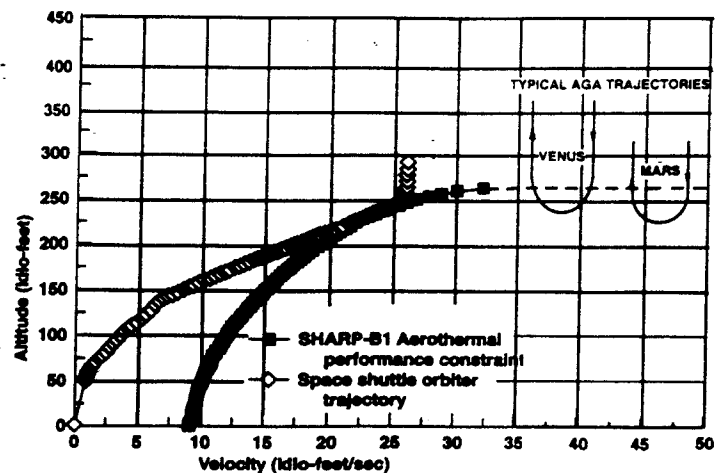


Fig. 9. Comparison between a Shuttle trajectory and a SHARP-B1 aerothermal performance constraint.